Journal of Marine Research, 68, 459–477, 2010

Influence of warm SST anomalies formed in the eastern Pacific subduction zone on recent El Niño events

by Dong-Kyu Lee[1,2] and Peter Niiler[1,3]

ABSTRACT

Anomalous April–June warm surface water in the eastern Pacific convergence zone (the Great Pacific Garbage Patch) subducts and depresses the thermocline as a single waveform. This waveform propagates toward the equator much more quickly (reaching the equator in 1.5–2.5 years) than the normal transit time (5–10 years) of the meridional overturning cell. The movements of the sea-surface temperature (SST) anomalies that occurred before the 1997 and 2009 El Niños can be clearly traced to the area south of 20°N using the altimeter sea-level signals. Upon arriving near the Pacific equator, these warm water anomalies can contribute to the formation of the El Niño by lowering the depth of the thermocline. The time required for a subducted SST anomaly to "drift" 3000 km to the equator depends upon its initial location and on the distribution of the SST anomalies near the western coast of North America. The subducted warm SST anomalies observed before the El Niños of 1982 and 1997 took 12 months to reach the equator. Longer drift times of 24 months were indicated for the 1972, 1986, 1993, 2003, 2006 and 2009 events. The thermocline depressions that "drift" toward the equator in the eastern Pacific are shown to be a major energy source for the onset of the El Niño in the central and eastern Pacific. This study presents a theory that could expand our understanding of the onset mechanism of the El Niño episode.

1. Introduction

The flattening of the equatorial thermocline causes a weakening of the Pacific Subtropical Cell (STC) and is known to have caused property changes in the El Niño-Southern Oscillation (ENSO) since the 1970s (McPhaden and Zhang, 2002; Yeh *et al.,* 2009). In this meridional overturning cell, both thermal energy anomalies and water are transported poleward in the surface layer (Fig. 1), subducted in the subtropics, transported toward the equator within the thermocline and upwelled in the equatorial region. The pathways for water parcels in the STC are either through the central Pacific or through the western boundary (Rothstein *et al.,* 1998). Transit times from subtropics (30°N) to the equator via the ocean interior path are about 5–10 years based on geostrophic velocity estimation (McPhaden and Zhang, 2002) and are about 4–6 years from bomb-produced radiocarbon (^{14}C) distribution (Quay *et al.,* 1983). Tritium observations by Fine *et al.* (1987) showed

1. Scripps Institution of Oceanography, University of California, La Jolla, California, 92093, U.S.A.
2. Corresponding author. ***email: lee@makaha.ucsd.edu***
3. Deceased

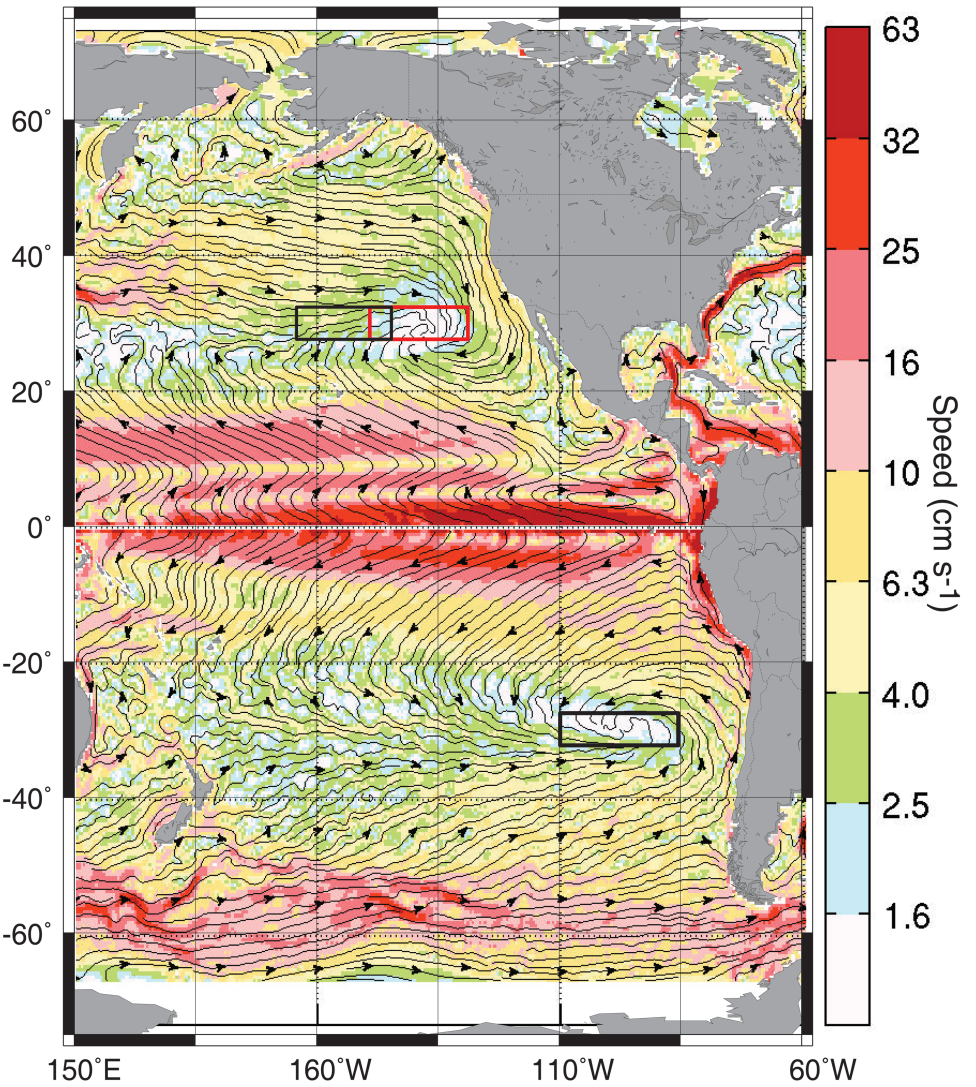

Figure 1. Areas used to calculate SST anomalies located in the area of whirlpool-type subduction zones. Stream lines calculated from combined mean geostrophic and Ekman velocities are from Maximenko *et al.* (2009). Red and black boxes in the Northeast Pacific are the areas of warm (1976–1999) and cold (1970–1975, 2000–2009) climate periods, respectively. The current speed is represented by color shading.

that the eastern equatorial upwelling zone received its tritium distribution from water that was subducted 10–14 years earlier north of 45°N in the eastern North Pacific. This overturning cell can play an important role in setting the northward scale of the El Niño pattern but can also contribute to the initiation of warming in the central and eastern

equatorial Pacific (McPhaden and Zhang, 2002). Since the thermal anomaly only needs to propagate energy rather than transport a water mass, it requires a shorter period of time to travel toward the equator than would be required by water transported by advection. From satellite-tracked drifter data, Niiler *et al.* (2004) have shown that the time-mean advections well outside of the equatorial waveguide determine the latitudinal scale of the sea-surface temperature (SST) anomaly. In other words, the poleward advection of thermal energy by the time-mean Ekman currents and the absorption of this excess energy by the atmosphere set the latitudinal scale of the El Niño SST anomaly, rather than the scales set by the waveguide dynamics. Here we continue to follow the concept that the eastern Pacific meridional overturning cell has a major role in developing the El Niño SST anomaly.

Occurrences of unusually warm SST anomalies (El Niño) or cold SST anomalies (La Niña) in the equatorial Pacific are phenomena that have global climate impacts. Numerous studies that examine different methods for predicting these anomalous conditions have been conducted, but some of the proposed dynamic mechanisms for the onset and evolution of these conditions seem to apply only to certain events (Cane *et al.,* 1986). A relaxation or reversal of the southeastern trade winds seems to be essential before the onset of an El Niño episode. One prevailing view is that the trade wind relaxation is part of a large-scale, coupled ocean-atmosphere dynamical system that oscillates between warm and cold phases. The triggering forces are due to boundary-reflected, equatorially-trapped waves in the ocean that are generated in the previous cold phase of strengthened trade winds (the delayed action oscillation theory: Battisti, 1988; Battisti and Hirst, 1989; Suarez and Schopf, 1988). A second theory involves the high-frequency intra-seasonal stochastic forcing that acts on the stable state of a cold ocean in the east and a warm ocean in the west, occasionally causing the trade winds to relax (Fedorov and Philander, 2000). After the wind relaxation occurs, Picaut *et al.* (1997) have reported that oceanic processes, such as the zonal current convergence of thermal energy in the central Pacific and equatorial waves reflected from the eastern boundary, are initiated and play fundamental roles in the subsequent development of an El Niño episode.

In the above theories, once the El Niño episode has been initiated, its further development on the equator appears to be well described in terms of linear and nonlinear oceanic as well as atmospheric dynamical elements. These elements are confined to the equator and have pronounced east to west movements in the equatorial wave-guide. The prognostic capacity for events initiated in these dynamically-based models extends SST predictions on the equator to 6–9 months (Jin *et al.,* 2008), which is considerably longer than statistical persistence. Using a coupled ocean-atmosphere model with SST assimilation, Luo *et al.* (2008) were somewhat successful in predicting the existence of equatorial SST anomalies up to 1.5 years, but the strength of the anomalies was not correctly predicted for the strong El Niño which occurred in 1997.

The calculation conveyed in the present work begins with the mean, near-surface particle displacements, or streamlines, calculated from surface velocity program (SVP) drifters and satellite sea-level data by Maximenko *et al.* (2009). Driven primarily by

Ekman forces, the streamlines converge at the centers of the subtropical basins, approximately 1000 km west of the respective eastern margins. The streamlines produce intensive convergent "swirls" at approximately 30°N and 30°S (Fig. 1). In the mid-thermocline, the most rapid time-mean equatorward geostrophic flows are the seaward extensions of the California and Chile-Peru Currents. The mid-depth flow is upwelled near the equator and completes an overturning cell that carries thermal energy between the equatorial and subtropical ocean (Shin and Liu, 2000; Solomon *et al.,* 2008) with transit time of 5–10 years (McPhaden and Zhang, 2002). This teleconnection between the tropics and subtropics at thermocline depths of the eastern Pacific allows for the slow transport of water particles. But a "wave-like" thermocline depression formed by the subduction of warm water can carry energy both through wave dynamics as well as through horizontal advection, and it can be propagated to the equator as a single wave without significant net mass transport. Thus, large amplitude thermal energy anomalies formed far from the equator in the eastern Pacific can be transported toward the equator on the time-mean eastern Pacific vertical cell, potentially affecting the onset and subsequent development of El Niño events. The tracking of thermal energy anomaly is more powerful than particle trajectory analysis for studying the El Niño because the El Niño is simply the surface expression of anomalous upper ocean heat content in the tropics. In the present study, we presents observational evidence of the formation of thermal anomalies in the mid-latitude eastern Pacific, well before the onset of an El Niño episode, and of their subsequent equatorward movements of thermal energy as a form of thermocline depression. These anomalies ultimately arrive near the equator at the onset of El Niño events. The present study gives a dynamical view of the theory that could potentially be used to predict an El Niño episode earlier than currently available dynamic and statistical models are capable of today.

2. Observations of SST anomalies in the eastern North Pacific

The 18-year (1990–2008) time mean paths of water particles at a 15-m depth, which were calculated from drifter and satellite sea-level observations by Maximenko *et al.* (2009), reveal patterns of poleward displacement in the tropical Pacific and whirlpool shape convergence zones (hereafter called drainage zones) in the mid-latitude eastern Pacific Ocean (Fig. 1). These distinct zones are regions of intense downwelling of near-surface water and are unique features that predominantly occur in the eastern Pacific. The physical characteristics of these zones have not been extensively studied because of their remote locations. Before the volunteer ship-of-opportunity (VSOP) XBT program started to sample sufficiently in the central North Pacific in 1970, density of temperature data was insufficient to map the three-dimensional thermal structure in the mid ocean (White and Bernstein, 1979). Thus, only observational data collected after 1970 were used in this study. After analyzing monthly SST anomalies from National Climate Data Center (www.ncdc.noaa.gov), springtime developments of warm SST anomalies over 1°C in the eastern North Pacific were found to occur as precursors of El Niño events. These anomalies

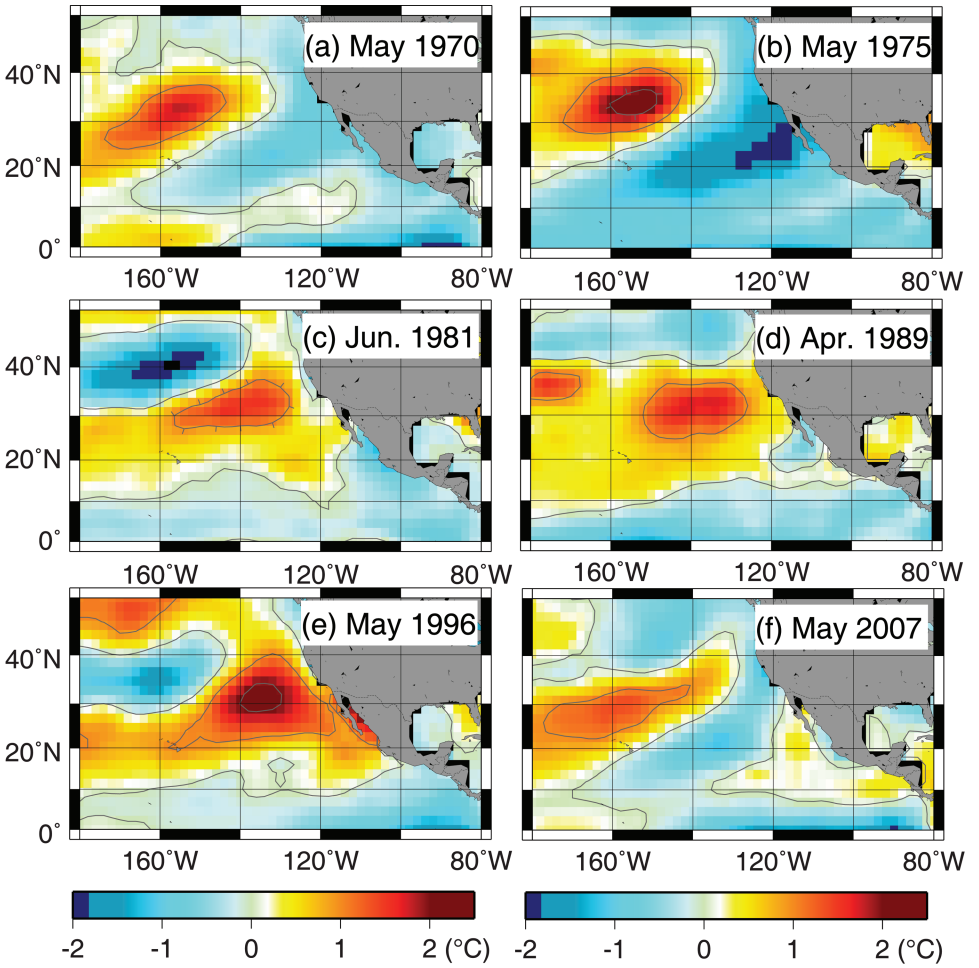

Figure 2. SST anomaly distribution in the eastern North Pacific on: (a) May 1970; (b) May 1975; (c) June 1981; (d) April 1989; (e) May 1996; and (f) May 2007.

appeared to be centered near or on the drainage zone (Figs. 2c, 2d and 2e) in the North Pacific during the warm climate phase of the North Pacific. As the wind and thermal energy exchange varies on large scales with the North Pacific climate phases (e.g., the North Pacific Oscillation), the longitude of the warm anomaly centers were shifted 15° to the west during the cool climate phase of the North Pacific before 1976 and after 1999 (Figs. 2a, 2b and 2f).

The monthly SST anomalies from January 1970 to March 2009 in the drainage zones in the eastern Pacific and in the Niño-3 region (90°W–150°W, 5°S–5°N) are presented in Figure 3. The areas used to calculate averages and determine monthly SST anomalies shown in Figure 3 were chosen based on the North Pacific climate phase (NPO) and they

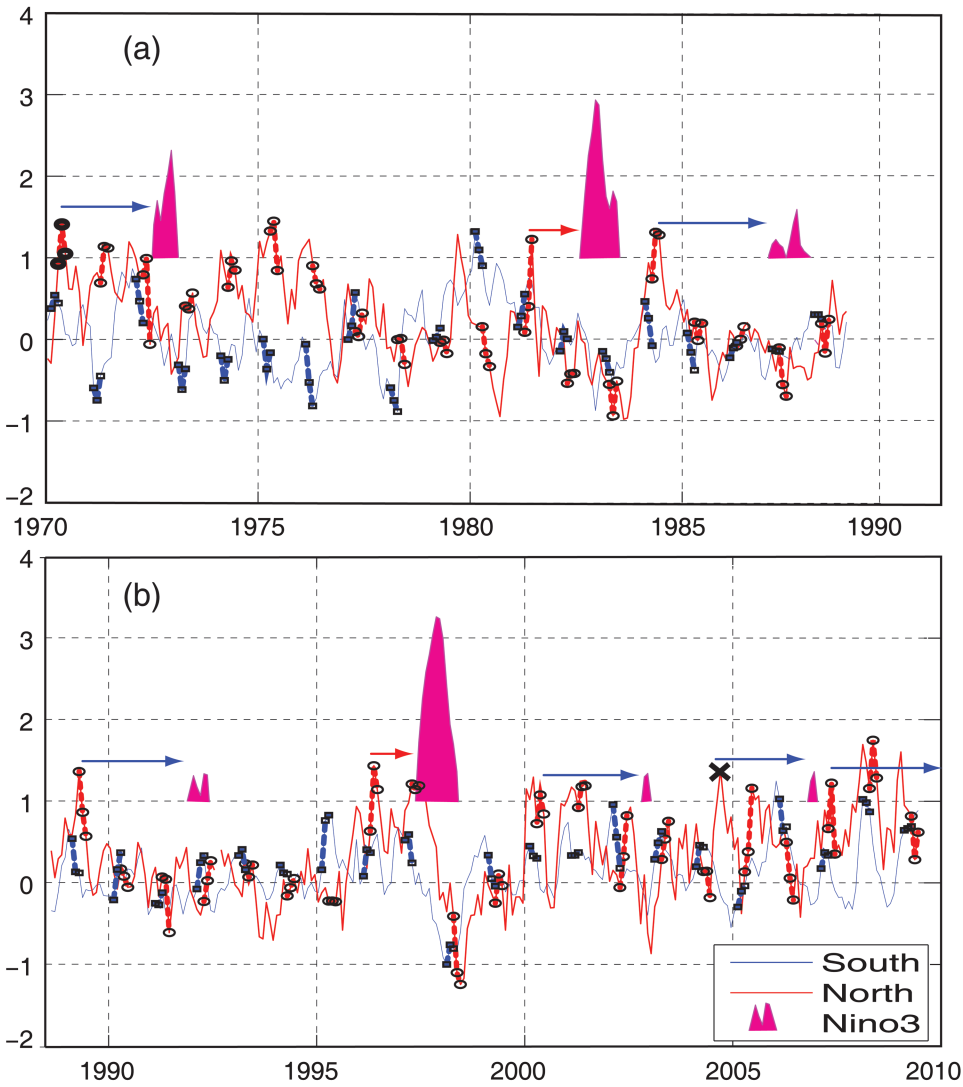

Figure 3. Monthly SST anomalies in the eastern Pacific for (a) 1970–1988 and (b) 1989–2010. In the North Pacific (thick red dotted red line with circles representing April–May–June), SST anomalies over 1°C led the El Niño episodes by 1.5 years (red arrows; 1982 and 1997) or 2.5 years (blue arrows; 1972, 1987, 1992, 2002 and 2006). A large northern SST anomaly in 2004 occurred in August (black cross). SST anomalies in the South Pacific (thick blue dotted line with squares representing February–March–April) played a supporting role to northern anomalies but were not directly related to the El Niño episodes. The Niño-3 SST anomalies over 1°C (red filled curves) are plotted only for El Niño periods.

are shown with a black box for the periods of cold phases and with a red box for the period of warm phase in Figure 1. Since 1970, there have been seven events of SST anomalies over 1°C in the Niño-3 region, and these can be classified into three groups depending upon the strength of the anomaly. First, the severe El Niño events with SST anomalies above 3°C occurred in 1982 and 1997. The El Niño that occurred in 1972 was a strong El Niño event with a SST anomaly over 2°C. The El Niño events in 1987, 1992, 2002 and 2006, which had SST anomalies above 1°C, were classified as moderate El Niño events. SST anomalies over 1°C in the northern drainage zone occurred in the northern spring (April–May–June) and it is shown in Figure 3 that they evidently occurred 18 months before the severe El Niño events or 30 months before moderate-to-strong El Niño events. The simple correlation analysis does not give a significant relationship between the monthly Nino-3 SST anomaly and the SST anomalies in the northern drainage zone (if they had significant correlation, it would have been discovered a long time ago). When only years of the SST anomalies in the northern drainage zone over a threshold anomaly over 1°C that occur in the April–May–June period were identified, and warm anomaly events on the equator in subsequent years were noted, every moderate-to-severe El Niño events since 1970 were accounted for (except for the August warm anomaly in 2004 that led to the 2006 El Niño). Two exceptions were found: (1) no development of an El Niño in 1975 and (2) 18 months lag-time between the northern anomaly and the El Niño development in 1983 and 1997. Both of these special cases will be discussed in more detail in the subsequent sections. The relationships we found from 8 El Niños (including the one in 2010) based on high quality large-scale thermal observations are robust enough to suggest that the theory for the eastern Pacific wave/advection contribution to the initiation of El Niño from the warm thermal mass in the northern drainage zone is indeed robust (especially if the exceptions referred to above can be dynamically rationalized).

SST observations suggest that large positive SST anomalies in the northern drainage zone may significantly contribute to the onset of El Niño episodes. As shown by Gu and Philander (1997), who analyzed connection mechanisms between the tropical Pacific and the subtropical Pacific using an ocean general circulation model, the equatorward propagation of warm anomalies in the eastern Pacific takes on an isopycnal form when lowering the thermocline. In the next section, we demonstrate the equatorward propagation of subtropical SST anomalies toward 20°N using sea-level and isopycnal anomalies that continue to surge their way directly onto the equator.

3. Formation and propagation of the subsurface warm anomalies

The teleconnection between the mid-latitude subduction of warm anomalies and the tropical SST anomalies in the Pacific has been noted before (Shin and Liu, 2000; Solomon *et al.,* 2008). For example, a subducted warm temperature anomaly was observed in the central North Pacific (near the 180°W), by Schneider *et al.* (1999), to move southwestward at a speed of 0.7 cm/s. However, the subducted warm features in the eastern Pacific (120°W–140°W) that were studied in the present work have not yet been reported. As the

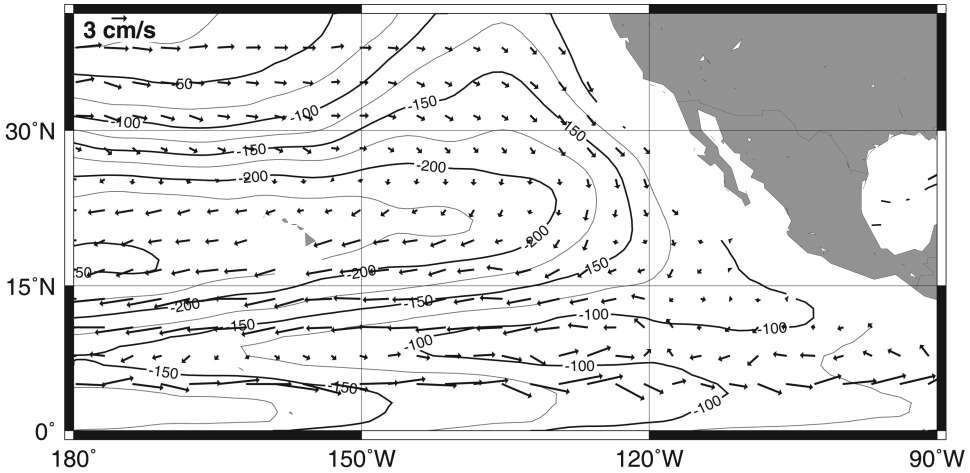

Figure 4. Mean geostrophic velocity (vectors) and mean depth (contour) of the $\sigma_\theta = 25.5$ surface in the eastern North Pacific.

potential density $\sigma_\theta = 25.5$ outcrops in our study area in the spring, the $\sigma_\theta = 25.5$ isopycnal surface was chosen for analysis in this work. We used the National Oceanic and Atmospheric Administration (NOAA) World Ocean Atlas 2005 (www.nodc.noaa.gov/OC5/WOA05) and the Global Ocean Heat Content (www.nodc.noaa.gov/OC5/3M_HEAT_CONTENT) to determine geostrophic shear and the depth of the $\sigma_\theta = 25.5$ isopycnal surface. The mean surface geostrophic currents estimated by Maximenko *et al.* (2009) from drifters, sea levels and gravity, as measured from satellites, were used as the reference velocities at the surface.

The mean geostrophic currents on the $\sigma_\theta = 25.5$ surface in the northern hemisphere (arrows in Fig. 4) showed a southeastward flow with a speed of 1–3 cm/s in the area near the northern drainage zone. The mean layer depth (contour lines in Fig. 4) of the $\sigma_\theta = 25.5$ surface was 130–200 m in the subtropical region and became shallower, reaching depths of less than 100 m, in the North Equatorial Current region south of 15°N. The mid-depth warm anomaly formed by the sinking of warm surface water was not easy to detect due to the scarcity of subsurface observations; however, a positive layer depth anomaly of a seasonal $\sigma_\theta = 25.5$ surface was identified using a deepened layer depth. To identify the warm concave depression formed by subducted warm water, the following process was performed: (1) potential density was calculated from a seasonal temperature anomaly and a mean seasonal salinity with the assumption that the formation of a warm depression is mostly developed by thermal energy; (2) layer depth anomalies were filtered using a low-pass filter with a cutoff wave number of $0.2^{\circ -1}$ to remove eddy-size features; and (3) the warm depressions were identified as having a zonal size of less than 10° and showing a southward propagation over the next several seasons (Fig. 5). The warm depressions were successfully identified most of the time, except in 1975 when a warm depression was

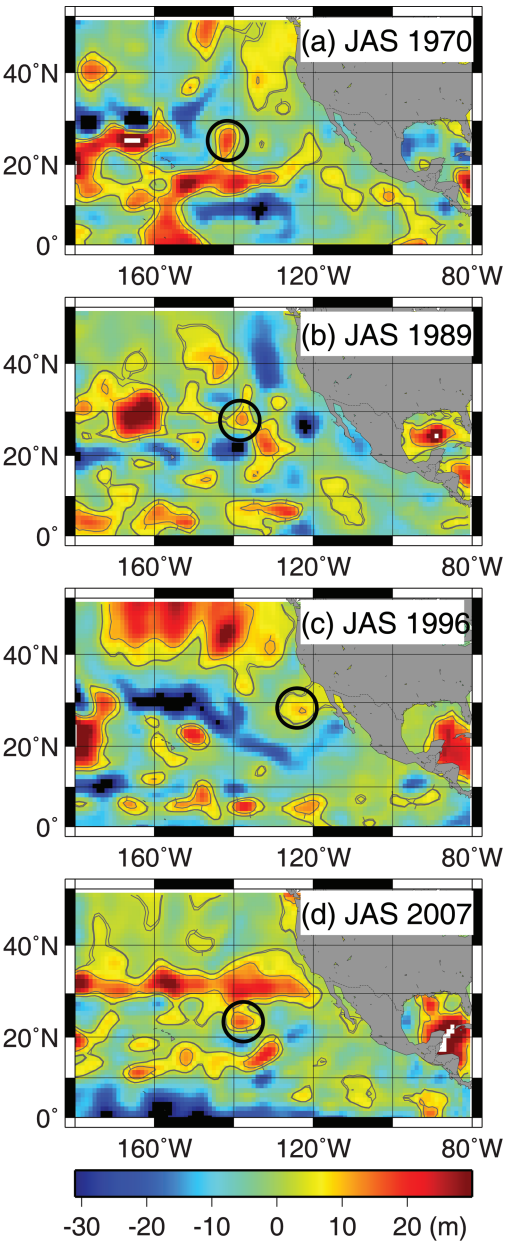

Figure 5. Seasonal (JAS: July–August–September) $\sigma_\theta = 25.5$ layer depth anomalies in the eastern North Pacific (contour lines at 3-m and 10-m anomaly depth). The subducted warm depressions are marked by black circles.

associated with the weak El Niño event in 1977. The center locations of the features associated with moderate and strong El Niños were clustered closely in the area of 136–141°W, 22–28°N (Figs. 5a, 5b and 5d) but those associated with severe El Niños (1982 and 1997) appeared to be farther to the east at approximately 121°W, 27–28°N (Fig. 5c).

The locations of warm depressions were overlaid on the location of the core of warm SST anomalies that depend upon the climate regime and the warm SST anomaly off the coast of Baja California. During the cold climate phase, a strong negative SST anomaly off the coast of Baja California in 1975 (Fig. 2b) prevented the formation of a noticeable warm depression in 1975. However, in 1970 and 2007, respectively, a near-normal SST (Fig. 2a) and warm anomaly (Fig. 2f) in the area off the coast of Baja California allowed a warm depression to be detected (Fig. 5a and Fig. 5d, respectively). A warm SST anomaly in the eastern North Pacific in 2007 was similar to that of 1970 and, based on the strength of the warm depression in 2007 and warm anomaly development in the area off the coast of Baja California, the 2009 El Niño was predicted here to be a strong event and the 2009 El Niño turned out to be the fourth strongest El Niño event since 1970. During the warm climate phase, when cold SST anomalies were observed off the coast of Baja California in 1984 (not shown) and 1989 (Fig. 2d), warm depressions were formed in the area near 140°W (Fig. 5b). The warm SST anomalies off the coast of Baja California in 1981 (Fig. 2c) and 1996 (Fig. 2e) caused a dramatic eastward shift in the depression that was formed as a result of a strong southeastward subsurface flow ($\sim$10 cm s^{-1}) within the $\sigma_\theta = 25.5$ surface as shown in Figure 6a. Temperature-salinity profiles revealed also that the warm and salty water in the subsurface layer centered at $\sigma_\theta = 25.4$ (the area marked with hatch pattern in Fig. 6b) intruded from the east.

Once subducted warm depressions were identified, they were tracked by their thermal anomaly signals, which produced a heightened sea-level anomaly. As variations in the thermocline depth mirrored the surface height in the simple two-layer system that is presented here, merged sea-level anomaly (SLA) data (ftp.cls.fr/pub/oceano/AVISO) were used to trace the propagation of warm depressions after seasonal- and eddy-scale variations were removed. The seasonal fluctuations of SLA at each grid were removed using harmonic analysis (Choi *et al.,* 2004) and low-pass filter with cut-off wave number of $0.2^{\circ -1}$ was applied to remove eddy scale fluctuations. The zonal basin-scale variations were also removed using a high-pass filter to remove basin-wide thermosteric effects (Chelton and Schlax, 1996). Positive sea-level anomaly features with an amplitude of approximately 5 cm that occurred near warm features identified in $\sigma_\theta = 25.5$ layer depth anomalies were found to propagate along the 123°W line in 1996 and along the 140°W line in 2007 (Fig. 7). These southward propagations were also verified with the $\sigma_\theta = 25.5$ layer depth anomaly data (not shown). The mean propagation speed was estimated to be approximately 7.5 cm s^{-1} in 1996, with a maximum propagation speed of more than 10 cm s^{-1} in August–October of 1996, and a mean propagation speed of 3.3 cm s^{-1} was estimated for 2007. When the depressions reached the North Equatorial Current region, they were joined

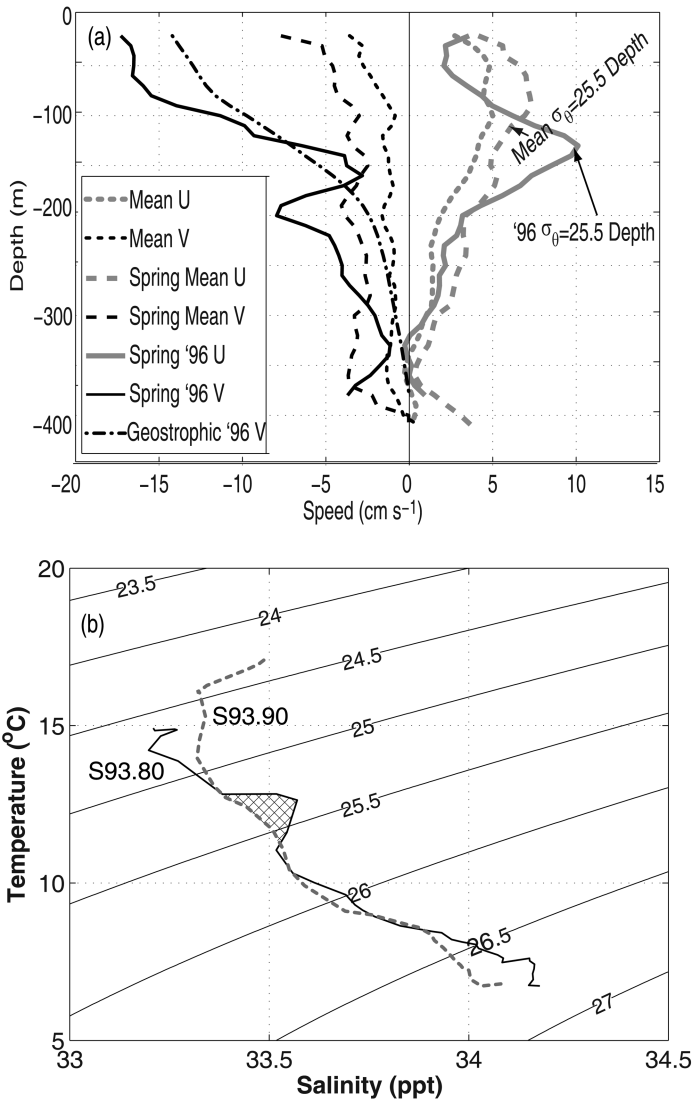

Figure 6. (a) The California Current observed on April 16–17, 1996 (black solid line for meridional velocity and gray solid line for zonal velocity) shown alongside the 10-year mean spring velocities (dashed lines) and of 10-year mean velocities (dotted lines) observed by an ADCP averaged over 120 km (marked as CalCOFI Line 93 in Fig. 7). Geostrophic current observed on April 17, 1996 at the core of the California Current is also shown by a dot-dashed line. (b) The Temperature-Salinity (TS) diagram of CalCOFI Line 93 Station 80 (S93.80; 31° 10.7′N, 120° 55.2′W) and Line 93 Station 90 (S93.90; 30° 50.8′N, 121° 35.2′W) observed on Apr. 17, 1996. The warm and salty water intrusion from the west is marked as hatch pattern.

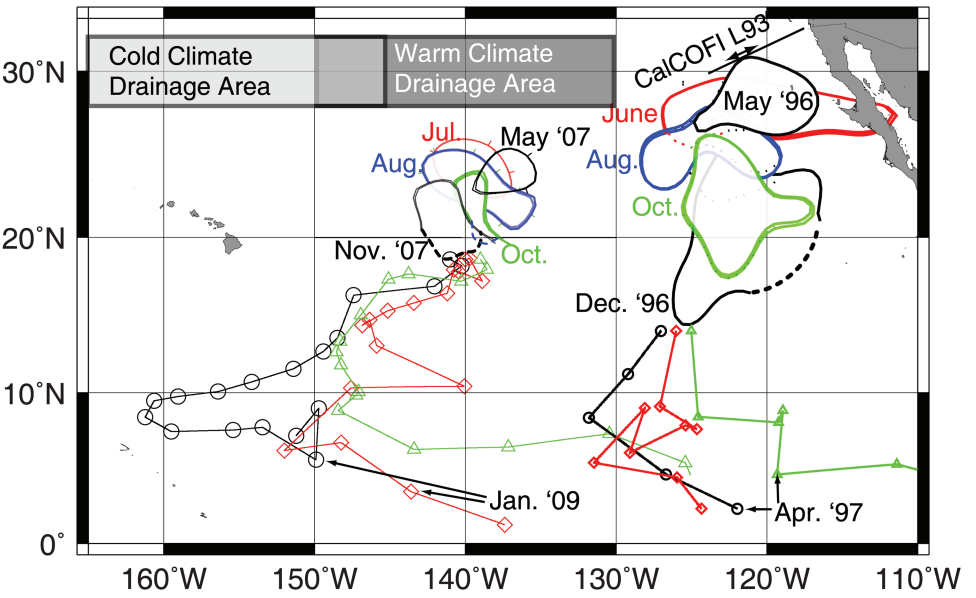

Figure 7. The equatorward propagation and tracks of subducted warm depressions observed in 1996–1997 and 2007–2009. The contours of the positive sea-level anomaly over 2 cm in magnitude are shown. The dotted lines indicate the boundary formed by other anomalies that propagated from the east. The starting locations of tracks were separated by 1° longitude and tracks were from particle traces using the absolute geostrophic velocities with a phase speed of 4 cm s^{-1} in 1996 and 2 cm s^{-1} in 2007. The monthly locations on the tracks are marked using symbols.

with other anomalies (dotted lines in Fig. 7) propagated from the east and were difficult to trace further in the sea-level data. Starting from the southern edge of the North Equatorial Current, the anomalous signals were tracked using geostrophic currents calculated from seasonal temperature anomalies added to the mean climate monthly temperature, after assumption that mostly thermal anomalies were involved in the propagation of this anomaly. This assumption was base on the fact that the anomaly in 2006 was not a density-compensated anomaly although it was warm and salty (see hatched area in Fig. 6b). The density difference between two stations aroused by subducted water was mostly accounted for by the temperature anomaly. The geostrophic currents were referenced relative to the absolute current at the surface, which was estimated from the mean dynamic topography by Maximenko *et al.* (2009), and to the monthly mean sea-level anomaly. The phase speeds of warm depressions were added to the geostrophic velocity and were estimated from the propagation speeds (7.5 cm s^{-1} for 1996 and 3.3 cm s^{-1} for 2007) of warm depressions in November–December after subtracting the mean geostrophic current (2 cm s^{-1} for 1996 and 1.3 cm s^{-1} for 2007) in the region. We assumed the constant phase speed when the warm depressions propagated to the equator after crossing

the North Equatorial Current. Because the baroclinic Rossby wave theoretically propagates faster in the tropics then in the subtropics (Chelton and Schlax, 1996), the phase speeds used here were the lower bound. The effect on estimating propagation path in the tropics using lower bound constant phase speed was far greater than the effect on estimating geostrophic advection assuming fixed salinity which would decrease the geostrophic current by anomalous warm temperature. The warm depressions arrived at the equatorial region at approximately 120–125°W in April 1997 and 130–150°W in January 2009 (Fig. 7). For the year 1997, the phase speed increase from 15°N to 3°N was greater than 5 cm s^{-1} (Chelton and Schlax, 1996) and the change of advection speed was about 0.3 cm s^{-1} on the $\sigma_\theta = 25.5$ surface (after assuming the maximum salinity increase of 0.2 psu; Fig. 6b). Thus the uncertainty of the estimated arrival time at the equatorial region caused by the approximation used in our study was less than 40 days.

4. Mechanisms

The presence of the eastern Pacific vertical cell has not been well-studied; however, northward mean surface currents in the central and eastern tropical Pacific have been observed by drifters (Fig. 1). When geostrophic currents referenced to the mean geostrophic surface current, which was estimated from drifters with altimeter and gravity data, were used to estimate geostrophic currents at the $\sigma_\theta = 25.5$ surface, mean southward geostrophic currents (Fig. 4) were found to prevail in the region south of 15°N. The equatorial upwelling of thermocline depth water is well known, but the drainage region or subduction zones in mid-latitudes have been only recently mapped from drifter and satellite altimeter observations. The connection between the tropics and subtropics at thermocline depths of the eastern Pacific allows for the slow transport of water particles, as demonstrated from a study tracing tritium from the Gulf of Alaska to the eastern equatorial Pacific (Fine *et al.,* 1987). However, the "wave-like" propagation in the meridional flow has not been previously discussed. The displacement of a thermocline anomaly can carry energy both through wave dynamics as well as through horizontal advection, both of which can result in thermocline depressions that can arrive at the equator as single waves without significant net mass transport. The thermocline is depressed by an arriving wave at the equator and this thermocline depression causes the upwelling of warm water at the upper limb of the shallow overturning cell, thus causing warm SST anomalies at the equator. This latter mechanism is akin to what equatorially-trapped Kelvin waves do as their thermocline depression propagates from the west.

When a large warm anomaly is formed in the area south or southwest of the drainage zone, it propagates with a phase speed of planetary motion and with the mean current. Linear baroclinic instability theory shows that the most unstable waves that draw energy from spiraling mean geostrophic shear near the eastern boundary of the mid-latitude North Pacific propagate to the south (Lee and Niiler, 1987). The southward-flowing California Current observed by Gay and Cherskin (2009) was strongest in the spring, with a mean speed of 8 cm s^{-1} at the surface (Fig. 6a), and was centered around 121°W with a width of

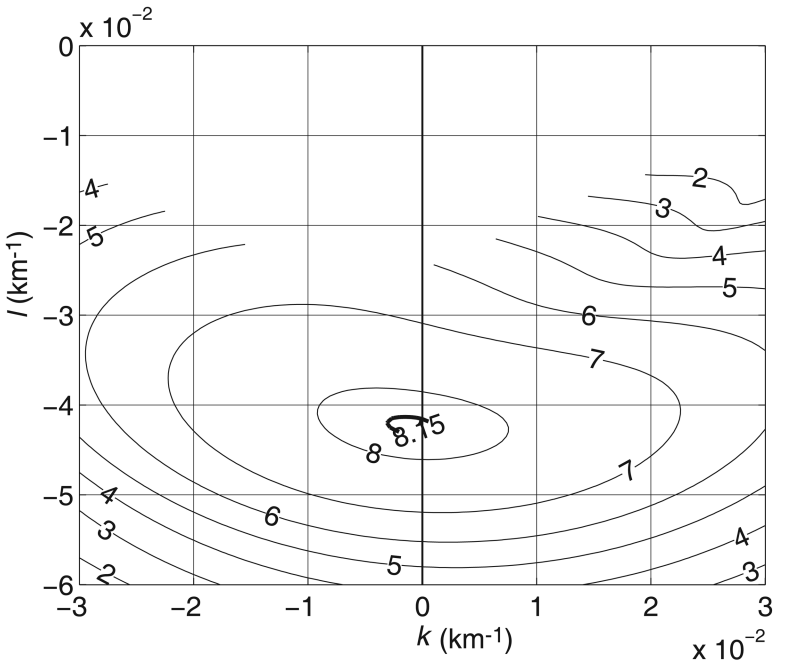

Figure 8. Linear growth rate contours of unstable waves with subsurface maximum amplitudes at 50–200 m depth (shown in units of 10^{-7} s^{-1}).

100 km. In 1996, the California Current observed both from an Acoustic Doppler Current Profiler (ADCP) and from geostrophic calculations showed a spring mean flow that was twice as large as that in spring of 1993–2003 (Fig. 6a). As the center of the observed warm depression in 1996 was near the core of the California Current (Fig. 7), the linear baroclinic instability calculation (Lee and Niiler, 1987) was performed using observed southward geostrophic shear in 1996. The region was unstable over a broad range of wavenumbers due to the strong mean meridional vertical shear of the California Current. The most unstable waves had maximum amplitudes at depths of 50–150 m and half wavelengths of 1500–3000 km (zonal) and 75–100 km (meridional) with a southward phase speed of 4.5–6 cm s^{-1} and an *e*-folding time of 15 days (Fig. 8). These baroclinically unstable waves had comparable length scales and phase propagation characteristics when compared with the observed warm depression in 1996. We do not have direct current observations for 2007 near the area of the warm depression; however, the most unstable waves from linear baroclinic instability by southwestward vertical shear in the eastern Pacific have approximately 1 cm s^{-1} southward phase propagation (Lee and Niiler, 1987), which is approximately half the speed of the observed phase speed for the warm depression in 2007. Recent observation of eddies (Chelton *et al.,* 2007) estimated from sea-level anomalies show phase speeds that are twice as large as those predicted by baroclinic instability theory. This enhanced propagation may also occur for baroclinic unstable waves traveling south. The

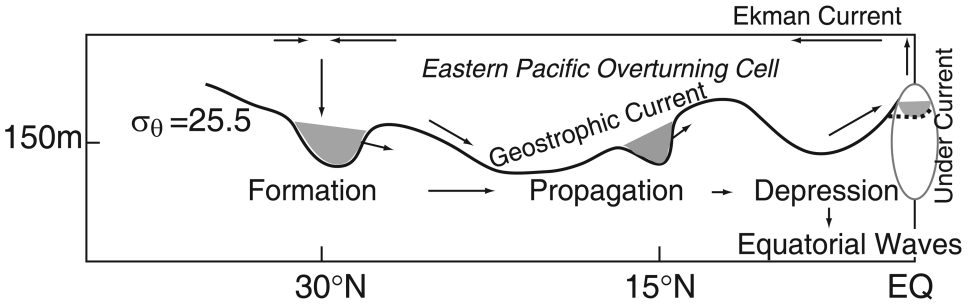

Figure 9. Concept of the eastern Pacific overturning cell and the onset of the El Niño episode by subducted warm depressions formed in the drainage zone. The warm anomaly moves equatorward with horizontal advection and phase propagation. When it arrives in the equatorial region, the depression deepens the thermocline and generates equatorial waves.

arrival of southward-propagating warm anomalies at the eastern equatorial region causes a depression of the thermocline and may trigger an equatorial Rossby wave, which deepens the thermocline in the central and eastern equatorial Pacific.

The weakening of east to west temperature gradient near the equator causes the trade winds to relax. Any process in the ocean which maintains the February–March small temperature gradient or which reduces the upwelling of cold water along the equator in the July–November period contributes to the development of robust El Niños. Lowering of the thermocline by the Kelvin wave propagated from the west or by the propagation of warm water anomalies to the equator in the eastern Pacific will contribute to the desired effect. Besides the phenomena in the equatorial wave guide, phenomena also in the eastern boundary advective/wave guide through mechanism shown here, contribute to the start and maintenance of El Niños. A further study using the complete Ocean General Circulation Model to simulate the observed phenomena shown in this paper is required to validate the theoretical suggestions presented above.

5. Discussions and conclusions

This paper describes the evolution of anomalous subducted warm surface waters in the eastern Pacific convergence zone in the spring as they grew into thermocline depressions as single waveforms. These subsurface anomalies propagated toward the equator rapidly, reaching the equator in 1.5–2.5 years, in comparison with the normal transit time of 5–10 years (McPhaden and Zhang, 2002) observed in the meridional overturning cell. After arriving at the equator, the thermocline depressions could be converted into major sources of energy to assist in the onset of El Niño events. The proposed mechanism for triggering ENSO via eastern Pacific anomalies is outlined in Figure 9. An anomalous warm depression is formed by the sinking of anomalous warm surface water in the northern hemisphere mid-latitude drainage zone of the eastern Pacific. After being subducted, this surface water propagates toward the equator as a single baroclinic unstable wave packet,

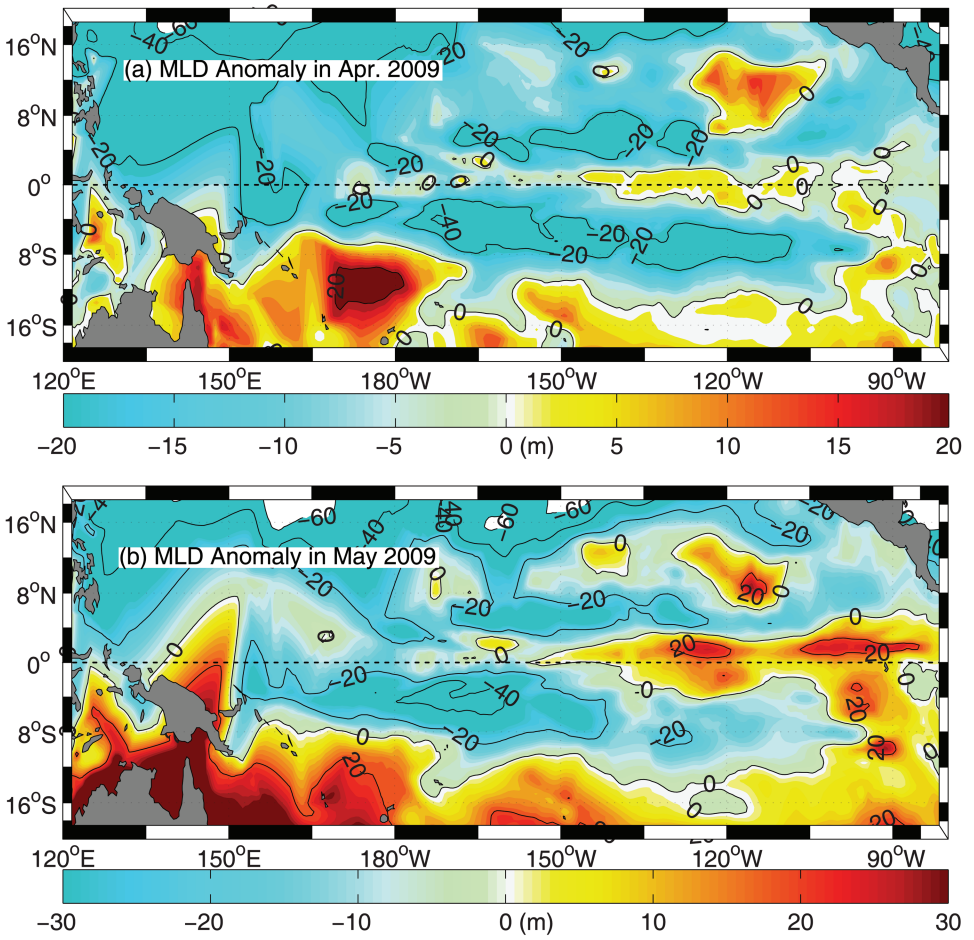

Figure 10. Mixed layer depth (MLD) anomaly (a) in April 2009 and (b) in May 2009 from Global Ocean Data Assimilation System (GODAS). Note that the deepening of the mixed layer for the 2009 El Niño originated in the north equatorial region (0–3°N, 120–135°W) in the eastern Pacific.

which continues to draw on the large available store of potential energy produced by the mean meridional shear of the thermocline circulation. When a positive SST anomaly is developed in the area off the coast of Baja California, the subducted warm water anomaly moves close to the American continent, and its southward propagation is faster because the southward shear and mean current are larger. Thus, warm depressions that were propagated along the pathway toward the equator and short transit times in mid-depth waters can cause the thermocline to be displaced to deeper depths in the equatorial region. Upon their arrival near the equator, these warm water anomalies lower the depth of the thermocline. As an example, the deepening of thermocline is shown using the mixed layer depth (MLD) anomaly in Figure 10 as the MLD anomaly generally follows the thermocline depth

anomaly in the eastern equatorial Pacific (McPhaden *et al.,* 2008). In spring of 2009, a deeper MLD than normal first appeared in the eastern Pacific (Fig. 10a), and the deepening of MLD was initiated in the equatorial North Pacific, not in the South Pacific (Fig. 10b). This early development of warming of upper layer in the eastern equatorial Pacific could also explain why the source of the El Niño event was found in the eastern equatorial Pacific instead of in the central equatorial Pacific (Picaut *et al.,* 1997).

All eight El Niños since 1970 were accounted for by the mechanism proposed in our theory. Exceptions (no El Niño and short time lag for severe El Niños) were also dynamically explained and shown in the data sets to be as plausible as the oscillator theories. Statistical analysis (i.e. maximum correlation with some lag in time) is not a robust method by which to view out theory, because we suggest that subducted warm depression needs a threshold anomaly over 1°C in the subtropical North Pacific that is strong enough to form the baroclinic unstable wave and to travel all the way to the equator along the eastern wave/advection guide. Our theory is in sharp contrast with theories that rely on linear motion within the equatorial wave guide. Our theory requires a significant interaction with the seasonal mean circulation of the eastern Pacific.

To further validate and refine the proposed mechanism, direct observations of subduction at the drainage zones, as well as numerical models that include features of the eastern Pacific overturning circulation cell, are needed. The formation of anomalous thermocline depression and the tracking of the energy propagation can be accomplished by deploying a moored Conductivity-Temperature-Depth (CTD) and current meter line at every 400–500 km along the expected path of propagation in the eastern Pacific, very much on the same scale of investment that is in the Tropical Atmosphere Ocean (TAO) array that now monitors the propagation along the equatorial wave-guide. It is worthwhile to note, however, that using only the SST anomaly data from the satellites in the eastern North Pacific, both the timing of El Niño and the strength of El Niño events can be correctly determined. The future El Niño events can be forecasted 1.5 years in advance for severe events and 2.5 years in advance for typical events. The dynamical explanations for the formation of a warm SST anomaly in the subtropical convergence zone and its occurrence only during the spring require further study and may provide further insight into the onset mechanism of El Niño episodes.

Acknowledgments. The second author of this paper, Peter Niiler, died on October 15, 2010. Through his Global Drifter Program, many new discoveries about ocean currents have emerged. Our work published here was inspired by the mid-ocean convergence zone observed from drifters. Not only was Peter a teacher, explaining the complexities of atmosphere-ocean dynamics in the simplest way, but he was also an art lover, house builder, professor and oceanographer. This great man will be deeply missed. This study was supported by NOO/CORC III at the Scripps Institution of Oceanography.

REFERENCES

Battisti, D. S. 1988. Dynamics and thermodynamics of a warming event in a coupled tropical atmosphere ocean model. J. Atmos. Sci., *45,* 2889–2919.

Battisti, D. S. and A. C. Hirst. 1989. Interannual variability in a tropical atmosphere ocean model—influence of the basic state, ocean geometry and nonlinearity. J. Atmos. Sci., *46,* 1687–1712.

Cane, M. A., S. C. Dolan and S. E. Zebiak. 1986. Experimental forecasts of El-Niño. Nature, *321,* 827–832.

Chelton, D., R. M. Samelson and R. A. de Szoeke. 2007. Global observations of large oceanic eddies. Geophys. Res. Lett., *34,* L15606.

Chelton, D. and M. Schlax. 1996. Global observations of oceanic Rossby waves. Science, *272,* 234–238.

Choi, B.-J., D. Haidvogel and Y.-K. Cho. 2004. Nonseasonal sea level variations in the Japan/East Sea from satellite altimeter data. J. Geophy. Res., *109,* C12028.

Fedorov, A. V. and S. G. H. Philander. 2000. Is El Niño changing? Science, *288,* 1997–2002.

Fine, R. A., W. H. Peterson and H. Gote Ostlund. 1987. The penetration of tritium into the tropical Pacific. J. Phys. Oceanogr., *17,* 553–564.

Gay, P. and T. Chereskin. 2009. Mean structure and seasonal variability of the poleward undercurrent off southern California. J. Geophys. Res., *114,* C02007.

Gu, D. F. and S. G. Philander. 1997. Interdecadal climate fluctuations that depend on exchanges between the tropics and extratropics. Science, *275,* 805–807.

Jin, E. K., J. Kinter III, B. Wang, C.-K. Park, I.-S. Kang, B. Kirtman, J.-S. Kug, A. Kumar, J.-J. Luo, J. Schemm, J. Shukla and T. Yamagata. 2008. Current status of ENSO prediction skill in coupled ocean-atmosphere models. Climate Dyn., *31,* 647–664.

Jin, F.-F. 1997. An equatorial recharge paradigm for ENSO: I. Conceptual model. J. Atmos. Sci., *54,* 811–829.

Lee, D.-K. and P. Niiler. 1987. The local baroclinic instability of geostrophic spirals in the eastern North Pacific. J. Phys. Oceanogr., *17,* 1366–1377.

Luo, J.-J., S. Masson, S. Behara and T. Yamagata. 2008. Extended ENSO prediction using a fully coupled ocean-atmosphere model. J. Climate, *21,* 84–93.

Maximenko, N., P. Niiler, M.-H. Rio, O. Melnichenko, L. Centurioni, D. Chambers, V. Zlotnicki and B. Galperin. 2009. Mean dynamic topography of the ocean derived from satellite and drifting buoy data using three different techniques. J. Atmos. Ocean. Tech., *26,* 1910–1919.

McPhaden, M., M. Cronin and D. McClurg. 2008. Meridional structure of the seasonally varying mixed layer temperature balance in the eastern tropical Pacific. J. Climate, *21,* 3240–3260.

McPhaden, M. and D. Zhang. 2002. Slowdown of the meridional overturning circulation in the upper Pacific Ocean. Nature, *415,* 603–608.

Niiler, P., D.-K. Lee and J. Moisan. 2004. Observed mechanisms of El Niño SST evolution in the Pacific. J. Mar. Res., *62,* 771–786.

Picaut, J., F. Masia and Y. du Penhoat. 1997. An advective-reflective conceptual model for the oscillatory nature of the ENSO. Science, *277,* 663–666.

Quay, P. D., M. Stuiver and W. S. Broecker. 1983. Upwelling rates for the equatorial Pacific Ocean derived from the bomb ^{14}C distribution. J. Mar. Res., *41,* 762–792.

Rothstein, L. M., R. H. Zhang and A. J. Busalacchi. 1998. A numerical simulation of the mean water pathways in the subtropical and tropical Pacific Ocean. J. Phys. Oceanogr., *28,* 322–343.

Schneider, N., A. Miller, M. Alexander and C. Deser. 1999. Subduction of decadal North Pacific temperature anomalies: observations and dynamics. J. Phys. Oceanogr., *29,* 1056–1070.

Shin, S. I. and Z. Y. Liu. 2000. Response of the equatorial thermocline to extratropical buoyancy forcing. J. Phys. Oceanogr., *30,* 2883–2905.

Solomon, A., S.-I. Shin, M. Alexander and J. McCreary. 2008. The relative importance of tropical variability forced from the North Pacific through ocean pathways. Climate Dyn., *31,* 315–331.

Suarez, M. and P. Schopf. 1988. A delayed action oscillator for ENSO. J. Atmos. Sci., *45,* 3283–3287.

White, W. and R. Bernstein. 1979. Design of an oceanographic network in the midlatitude North Pacific. J. Phys. Oceanogr., *9,* 592–606.

Yeh, S.-W., J.-S. Kug, B. Dewitte, M.-H. Kwon, B. Kirtman and F.-F. Jin. 2009. El Niño in a changing climate. Nature, *461,* 511–514.

Received: *24 February, 2010;* revised: *24 August, 2010.*